Nickel Electrodeposition on a Gold Polycrystalline Foil: A Combined Voltammetric and Photoelectron Spectroscopy Study

Spiridon Zafeiratos,* Fotis E. Paloukis, and Stylianos G. Neophytides

Institute of Chemical Engineering and High Temperature Chemical Processes, ICEHT-FORTH, P.O. Box 1414, GR-26504, Patras, Greece

Received: June 25, 2003; In Final Form: November 12, 2003

Cyclic voltammetry (CV) and X-ray and UV photoelectron spectroscopy (XPS, UPS) were employed to study the electrochemical deposition and dissolution of nickel on a polycrystalline gold electrode, in a 0.1 M $NiSO_4$ electrolyte. The modification of the Ni/Au interface upon thermal treatment in ultrahigh vacuum was also investigated. Depending on the applied potential, two distinct Ni chemical states were observed. At −0.5 V versus SCE an oxidized Ni phase, mainly $Ni(OH)_2$, was formed, whereas at potentials lower than −0.8 V nucleation of reduced Ni species surrounded by hydroxidized nickel occurred. The systematic investigation of the adsorbate species binding energies as a function of the applied potential revealed that hydroxidized nickel precipitates on the gold electrode, while reduced nickel species directly deposit on the electrode surface via the reduction of Ni^{2+} ions. Heating the Ni/Au interface to 650 K decomposes the adsorbed nickel film forming a new compound containing a Au−Ni intermetallic component.

1. Introduction

Bimetallic electrodes have received increasing interest in recent years because of their importance in a vast number of applications, including fuel cell catalysts and coating technology.[1] The investigation of such systems, using combined electrochemical and surface science experimental methods, provides a powerful tool to get chemically specific information about the intermetallic interface formed by electrodeposition.[2] The electrochemical deposition of nickel itself is an important well-established technical process that requires an improved control of the structure and the morphology of the Ni deposit and of the deposition process. In previous studies of Ni electrodeposition on carbon and various metallic substrates, a deposition mechanism was derived using electrochemical methods. According to this mechanism, first Ni_{aq}^{2+} ions in the solution are reduced to adsorbed Ni_{ad}^{2+} species, followed by the deposition of metallic Ni^0 on the substrate.[3,4] However, electrochemical investigations yield only indirect information about nickel adlayer chemical state and therefore further characterization is required. Photoelectron spectroscopy, perhaps the most promising technique for this endeavor, has been used in studies of the electrochemical double layer in ultrahigh vacuum systems.

Nickel deposition on gold electrodes has been studied previously by X-ray adsorption near-edge structure (XANES),[5] electrochemical methods (CV, EQCM),[6] and combined in situ scanning tunneling microscopy (STM) and cyclic voltammetry techniques.[7−10] These studies were focused mainly on low index single crystal Au substrates, studying in situ the oxidation state of nickel adsorbate, as well as its structural morphology and the role of the Au surface structure. An extensive in situ STM study of the initial stages of Ni electrodeposition on various Au single crystal surfaces shows that the nucleation of Ni adlayer depends strongly on Au surface morphology. For example, Ni deposition on Au(111) proceeds in three different nucleation steps, in connection with the applied overpotential.[8] The underpotential deposition of nickel on Au(111) seems to depend strongly on the ion species of the electrolyte. Ni underpotential deposition on Au(111) can be promoted in sulflamic (H_2NSO_3H) solutions[10] in contrast to Watts bath or sulfate solutions, where underpotential deposition was not observed.[9] Furthermore, the electrocatalytic activity of a chemically modified electrode composed of nickel film on a gold substrate was investigated recently in an alkaline medium using glucose as a model compound.[11] The results showed a strong catalytic activity of modified gold electrodes over a wide range of applied potentials.

In this work, we present combined photoelectron spectroscopy and electrochemical study of nickel deposition on gold. Deliberate use of a polycrystalline Au foil, with definite amounts of carbon and oxygen on the surface, was made, so as to mimic more closely the properties of practical electrodes used in electrochemical applications. The objective of this study is to identify the chemical state of Ni species and the structure of the double layer formed in the context of their role in important applications in batteries, electrochromic devices, and catalysts. Therefore, after electrochemical deposition, the sample was exposed to laboratory atmosphere to detect changes in the electrochemical double layer induced after exposure. It has been shown previously that the double layer remains structurally intact at the electrode upon its emersion from the solution over a wide range of conditions.[12] In this respect, the emerged electrode remains electrochemically active after emersion and the discharge of the double layer is accompanied by the exchange of species with its surrounding environment.[13] This procedure is expected to have an effect on the chemical state of the intermetallic interface. An extended vacuum characterization of the interface as well as a thermal treatment in UHV were carried out with the aim of elucidating the physicochemical properties of the Ni−Au interface.

* Corresponding author. Tel.: +30 2610 965261; fax: +30 2610 965223; e-mail address: spizaf@iceht.forth.gr.

10.1021/jp035804q CCC: $27.50
Published on Web 12/30/2003

2. Experimental Section

Polycrystalline gold foil (Alfa 99.994%) of a 1 cm^2 surface area was used as the working electrode material. Prior to electrodeposition, traces of oxygen and carbon could be detected on Au substrates as checked by XPS. Those impurities were easily removed in UHV by mild ion bombardment and subsequent annealing at 700 K. However, carbon contamination (mainly hydrocarbon-like species) was re-absorbed on the substrate, during sample transfer from the electrochemical cell to the UHV chamber because of air exposure in the laboratory environment. This amount was deliberately left on the electrode surface, even though a detailed description of the surface condition just before electrochemical measurements is difficult because of the presence of solvent ions and water molecules, forming the electrochemical double layer.[2]

An alternative procedure of electrode transfer was used to check the influence of laboratory atmosphere exposure to chemical state of electrodeposited nickel. Thus, electrochemical experiments were also performed inside an inert atmosphere glovebag, which was attached to the surface-analysis chamber. In this procedure after emersion of the electrochemical cell, the electrode was transferred to the UHV chamber under ultrapure nitrogen gas atmosphere at ambient pressure.

The deposition of Ni on Au was carried out potentiostatically in an electrolyte solution containing 0.1 M $NiSO_4$ (pH = 5.9). The electrolyte solution was prepared from Millipore (Milli-Q) grade water using analytical grade reagents and prior to use was purged with 99,999% nitrogen, to remove dissolved gases. Electrochemical measurements were performed at room temperature in a conventional three-electrode electrochemical cell with a saturated calomel electrode (SCE) as reference electrode and a Pt-wire as counter electrode. An EG&G model 263A potensiostat-galvanostat was used for the electrochemical measurements. All electrode potentials in this work are referred to the potential of the saturated calomel electrode (SCE). After electrochemical experiments, the samples were thoroughly rinsed in Millipore water, dried in a nitrogen stream, and immediately transferred to the UHV chamber for further analysis.

The photoelectron spectroscopy experiments were performed in an ultrahigh vacuum (UHV) chamber (base pressure 8×10^{-10} mbar), equipped with a hemispherical electron energy analyzer, a twin anode X-ray gun, and an UV lamp.[14] The unmonochromatized Al Kα line at 1486.6 eV and a constant pass energy mode for the analyzer were used in the XPS experiments. Pass energy of 97 eV resulted in a full width at half-maximum (fwhm) of 1.8 eV for the Au $4f_{7/2}$ peak of a reference foil. The He II line at 40.8 eV was employed for UPS measurements. The energy scale of the spectrometer was calibrated with both the Au $4f_{7/2}$ line at 84.0 eV and the Ni $2p_{3/2}$ line at 852.4 eV of carefully cleaned polycrystalline Au and Ni foils, respectively. The sample temperature was measured with a Ni−CrNi thermocouple, which was mounted in the sample holder. Curve fitting was performed with a least-squares curve fitting program based on a mixed Gaussian/Lorentzian function, which accounted for the band asymmetry at higher binding energies in the core level spectra of metallic species.

3. Results

3.1. Electrochemical Measurements. Nickel overlayers were deposited on polycrystalline Au foil, at a constant potential application, from a 0.1 M $NiSO_4$ solution, at 25 °C. The electrodeposition was characterized primarily by cyclic current−voltage curves (cyclic voltammograms), in the range of 0.6 and −0.85 V versus SCE. A typical voltammogram obtained from a fresh Au electrode is shown in Figure 1. The cycle commenced at 0 V toward −0.85 V, reversed at +0.6 V, and terminated at 0 V. As the potential changes from the region where no deposition is observed (0 V vs SCE), to the region where Ni deposition is expected to take place (ca. −0.6 V), a cathodic current flows because of the charge-transfer processes involved. The predominant feature in the cathodic potential sweep is a large negative current density which can be due to both Ni deposition and parallel hydrogen evolution, according to previous results of Ni electrodeposition on Au(111) in Watts bath electrolyte.[9,15] A broad peak located at ca −0.5 V (indicated as a_1), appears to be consistent with the onset of Ni deposition, as observed previously.[9] Upon potential reversal, an increasing current density is observed, giving rise to a stripping peak at −0.2 V (indicated as a_2), in the potential region where Ni dissolution peak has been reported, for several cases including Ni on Au(111).[5,9,15] In subsequent potential cycles, the voltammogram is completely reproducible, suggesting that the electrode surface is not altered significantly by deposition and stripping of Ni.

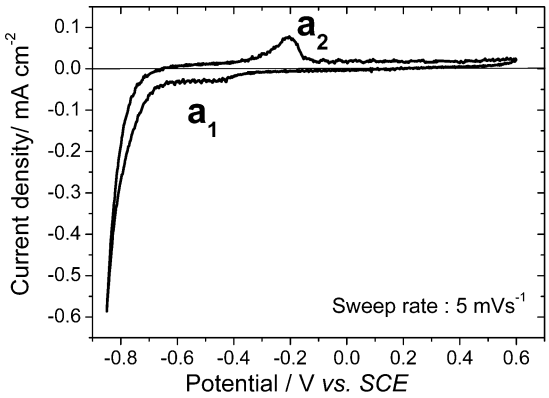

Figure 1. Cyclic voltammogram obtained at Au electrode in 0.1 M $NiSO_4$ electrolyte. Sweep rate 5 $mV \cdot s^{-1}$.

The amount of deposited Ni is assessed by applying a cathodic potential at a fixed value for a period between 15 and 120 s. Subsequent scans into the Ni desorption region produce sets of peaks that increase with applied potential duration. In Figure 2a and b, representative current−potential curves are presented for two holding periods of 120 and 15 s, respectively, at three characteristic hold potential values, namely, −0.52, −0.58, and −0.65 V. It can be observed that the anodic curve peak heights, as well as the number of dissolution peaks, are influenced by applied potential. At the lowest potential (−0.52 V), only one broad anodic peak centered at about −0.05 V is seen in Figure 2. Upon increasing potential toward more negative values (−0.58 V), the dissolution peak becomes wider and its maximum moves toward more cathodic potential. The origin of the peak broadening seems to be a second more intense peak at ca −0.35 V, which is becoming dominant at more cathodic applied potentials. The presence of two dissolution peaks observed in Figure 2 suggests the probable existence of several nickel chemical states formed at the gold electrode/electrolyte interface. This is consistent with previous results of nickel stripping from polycrystalline gold and vitreous carbon electrodes.[16,17]

Figure 3 shows the time dependence of the total anodic charge density for a given polarization potential obtained from experiments similar to those of Figure 2. The total charge is calculated by the integration of the anodic stripping peak area (corrected for double layer charging), which is directly related to the amount of nickel dissolved from the electrode surface.[9] It was

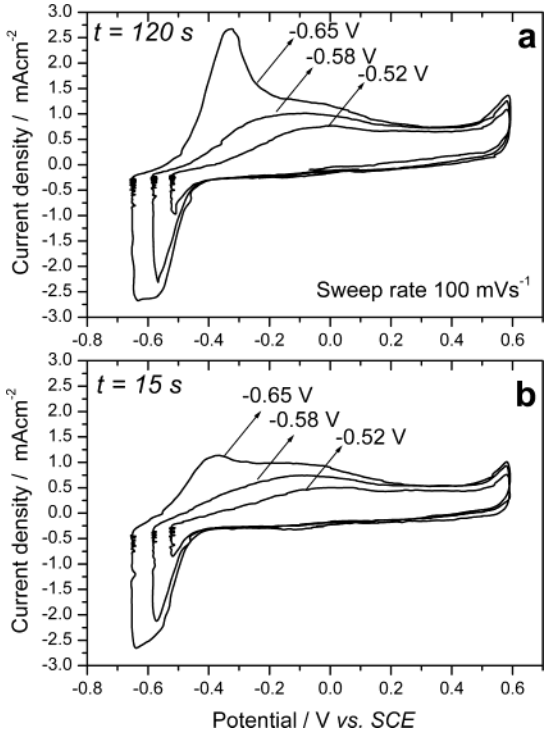

Figure 2. Cyclic voltammograms of Au in 0.1 M $NiSO_4$ electrolyte after potential sweep and subsequent (a) 120 s waiting period at −0.52, −0.58, and −0.65 V and (b) 15 s waiting period at the same potentials (sweep rate 100 $mV \cdot s^{-1}$).

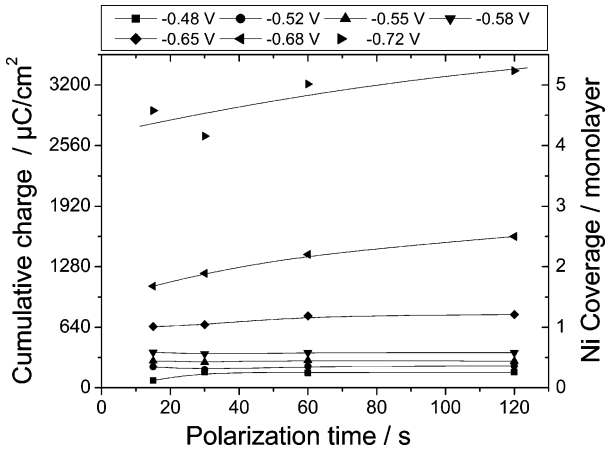

Figure 3. Electrochemical charge of anodic CV curves as a function of polarization time for various cathodic potentials. The right *y*-axis represents the estimated Ni coverage at equivalent monolayers derived from the charge of the Ni dissolution peak.

not trivial to obtain an accurate coulometric measurement of the amount of deposited nickel from the cathodic region because of the simultaneous evolution of hydrogen gas in this potential region that caused large fluctuations in the current density. The nominal Ni coverage shown on the right *y*-axis of Figure 3 was calculated from the total charge, assuming that the entire anodic charge can be attributed to the Ni dissolution reaction transferring two electrons per Ni atom. The surface concentration of one Ni monolayer is roughly equal to 2×10^{15} atoms$\cdot$cm^{-2}, corresponding to a charge density of 640 μCb$\cdot$cm^{-2}. The anodic charge in Figure 3 (thus Ni atoms deposited), exhibits a linear increase with decreasing applied potential. In contrast, nickel coverage remains constant (±5%) in the range of −0.48 to −0.58 V, with increasing polarization time, but increases with time at potentials more negative than −0.65 V.

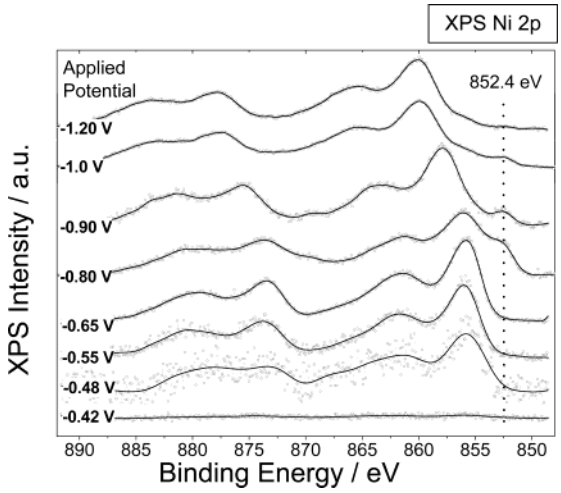

Figure 4. XP spectra of the Ni 2p core level for a Au polycrystalline electrode immersed and emersed from 0.1 M $NiSO_4$ electrolyte at various potentials.

3.2. Measurements in UHV Chamber. *3.2.1. XP Spectra of Deposited Nickel.* The examination of the chemical state of nickel deposited on the electrode surface was accomplished by photoelectron spectroscopy. After electrochemical measurements, the sample was emersed from the cell and the traces of the remaining solution on the surface were removed by rinsing with Millipore water. Thereafter, the sample was placed on the sample holder and introduced into the UHV chamber, for subsequent analysis. The rinsing procedure is expected to remove the salts of the electrolyte solution so that they will not remain on the electrode surface after water evaporation. In this respect, only the double layer and chemisorbed species will remain on the surface.[18,19] To ensure that no nickel adsorbs on the electrode at open-circuit potential, a clean Au foil was transferred to the electrochemical cell and immersed in the solution (at open-circuit potential) for 10 min. XPS examination of the sample after rinsing with Millipore water and transfer back to the UHV chamber showed slight contamination by oxygen and carbon, but no other detectable species. Thus, it can be considered that all Ni species detected by XPS and UPS experiments described below are deposited on Au surface because of potential application.

Figure 4 shows a set of Ni 2p spectra recorded on gold electrodes after 15 s of immersion at various potentials in a 0.1 M $NiSO_4$ solution. Spectras have been normalized to the same height so that differences of spectrum line features can be more pronounced. The Ni $2p_{3/2}$ binding energy (BE) measured increases as a function of the applied potential from 855.6 (±0.1) eV at −0.48 V deposited Ni up to 860.2 eV for the highest applied potential (−1.2 V). Similar binding energy shifts were observed for C 1s and O 1s peaks, too. A significant observation in Figure 4 is the appearance of a new component of the Ni 2p peak at lower BE which is visible at applied potentials below −0.8 V. This new component (for brevity called Ni^0) centered at 852.4 eV is still evident, although attenuated, at cathodic potentials less than −1 V. Its BE is independent of the applied potential, in contrast to the main Ni 2p peak, which shifts toward higher energies.

In Figure 5, we present the BE of Ni $2p_{3/2}$ peak as well as the ratio (I Ni 2p/I Au 4f) of the XPS intensities of the Ni 2p and Au 4f core levels as a function of the applied potential. The Ni/Au intensity ratio is indicative of the Ni coverage on the electrode, that is, larger ratios correspond to higher nickel coverages. On the basis of the Ni/Au intensity ratios, it is evident

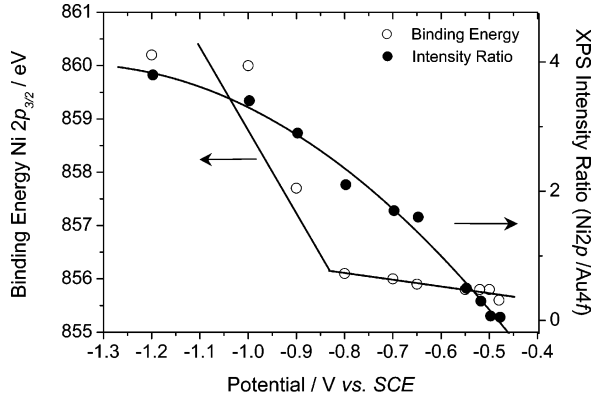

Figure 5. The XPS Ni $2p_{3/2}$ binding energy (○) and Ni 2p/Au 4f intensity ratio (●) plotted as a function of electrochemical emersion potential.

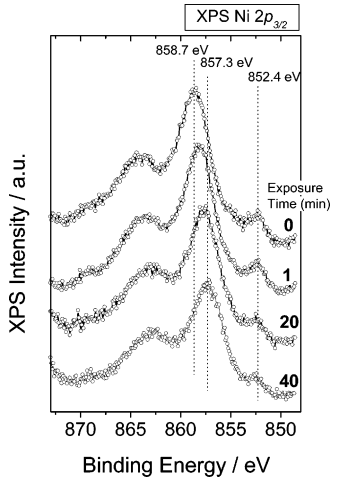

Figure 6. XP spectra of the Ni $2p_{3/2}$ core level for a Au polycrystalline electrode emersed at −0.9 V vs SCE from a 0.1 M $NiSO_4$ electrolyte and transported in UHV chamber under inert atmosphere, as a function of subsequent air exposure time.

that the degree of nickel uptake increases when applying more negative potential. These results indicate that nickel adsorption is controlled by the applied potential, in agreement with the electrochemical measurements presented above. In addition, the BE of the Ni 2p peak also exhibits a clear potential dependence. Over a potential range between −0.5 to −0.8 V, a good linear correlation of BE and applied potential is obtained with a slope close to unity. However, a significant increase of the BE is observed after −0.8 V, which is accompanied with an increase of the overall peak width.

The binding energy shift of Ni 2p, as well as of O 1s and C 1s peaks by varying emersion potential, suggests the lack of electronic equilibrium between deposited Ni and the substrate. The interpretation of BE shifts in bulk oxide compounds has been connected to the fact that the use of electron-based spectroscopic techniques on insulating materials leads to surface charging.[20,21] However, this problem is less pronounced for thin oxide films on conducting substrates because of tunneling effects. In addition, the observation of systematic BE shift of the double layer constituents as a function of the applied potential has been reported before for emersed electrodes.[22] Thus, the increase of nickel BE at potentials up to −0.8 V is consistent with the increase of the applied overpotential, while for more cathodic potentials charging effects are dominant, probably because of increased thickness of the adlayer.

Correcting the energy scale using C 1s peak of adventitious carbon species adsorbed on nickel adlayer (at 284.6 eV) as an intrinsic reference gives a binding energy of 855.4 ± 0.2 eV for the dominant Ni $2p_{3/2}$ peak, independently of the applied potential. Binding energies at 855.4 eV indicate the presence of Ni species in the form of Ni^{x+} ions. The binding energy of Ni $2p_{3/2}$ associated with $Ni(OH)_2$ thin films prepared on polycrystalline Ni foils in UHV, as well as electrochemically prepared γ-NiOOH powder, was found typically at 855.5 and 855.3 eV, respectively.[20,21,23,24] In addition, an intense shake-up structure is pronounced at 5.7 eV higher energies than the main Ni $2p_{3/2}$ peak in both cases.[21,24] According to those reports, our data is consistent with nickel−hydroxide and oxyhydroxide compounds. However, the formation of oxyhydroxide compounds is unlikely since those species are formed only at anodic potentials.[25] However, this assignment is not straightforward since other oxidized nickel forms, for example, ultrathin NiO films, can account for the measured BEs.[26] Nevertheless, the assumption of hydroxide formation is further confirmed by O 1s XPS signal (see section 3.2.2). The correction of Ni 2p binding energy by the use of C 1s peak as a reference is not applicable for the small Ni 2p peak centered at 852.4 eV, of which the binding energy remains constant with increasingly applied electrode potential. This remark is related to the arrangement of the nickel film and it will be discussed later.

Another important issue that must be addressed is the possible chemical interactions on the electrode when it is exposed to the ambient atmosphere during the emersion and transferring in UHV chamber. Nickel depositions on various potentials were repeated, this time transferring the sample under an inert gas atmosphere. Figure 6 shows characteristic spectra of Ni $2p_{3/2}$ peak for a Ni/Au electrode prepared at −0.9 V and transferred under nitrogen atmosphere in UHV. The peak shape as well as its main features does not change as compared to the air-exposed sample (see Figure 4). The difference is specified in the binding energy of the main peak, which in inert atmosphere exhibits a 0.9 eV shift toward higher energies, as compared to the corresponding binding energy of the Ni 2p spectrum at −0.9 V in Figure 4. After subsequent exposures of the sample to air, Ni $2p_{3/2}$ as well as O 1s and C 1s binding energies shift toward lower energies, while the BE of the small Ni peak is unaffected and always remains fixed at 852.4 eV. The air exposure of the sample is also accompanied by a pronounced attenuation of Ni 2p line intensity as well as with an increase in the signal of the C 1s region.

3.2.2. XP Spectra of Oxygen Species. The oxygen 1s band was studied in an attempt to obtain more clues about the coadsorbed species on the electrode surface. XP spectra for the energy range of O 1s are shown in Figure 7 for Ni deposition at various applied potentials. The binding energy scale is corrected using adventitious carbon species (binding energy at 284.6 eV) as an internal reference. A line shape analysis using a standard fwhm (2.2 eV) of O 1s peak shows that in all cases the O 1s signal could be decomposed in two components, with fixed binding energies. However, the relative intensity ratio of those components varies upon potential changes. Although a safe assignment of the O 1s bands is generally difficult for electrochemical systems, the consistency of peaks position and intensity in the line shape analysis indicates that contribution from two oxygen-containing species is likely to exist in the overall spectrum. An O 1s binding energy of 531.7 ± 0.1 eV is typical for OH or OOH species.[24,27] The binding energy of 533.2 ± 0.2 eV for the second O 1s peak component is characteristic of oxygen in H_2O.[28,29] Like the Ni 2p peak, the O 1s peak width for more cathodic applied potential than −0.8 V was broadened considerably, probably because of intense electrostatic charging

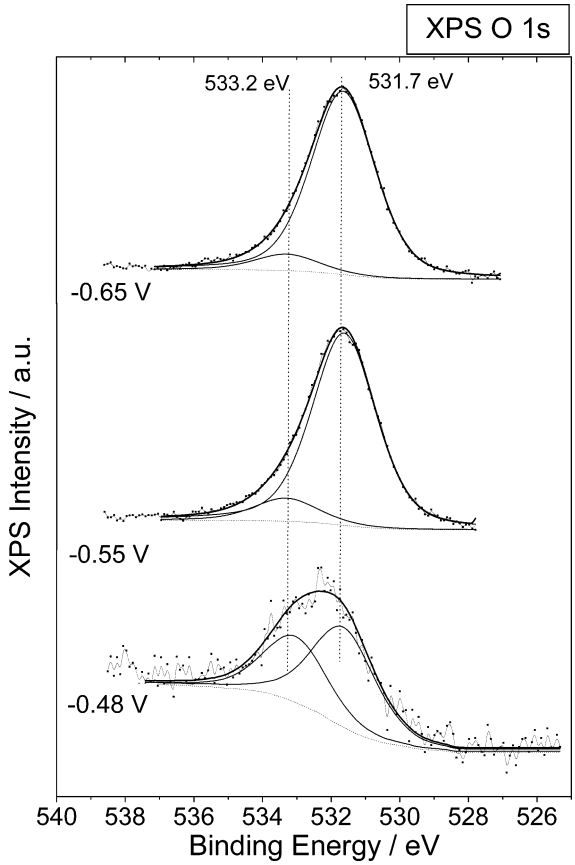

Figure 7. XP spectra of the O 1s core level for a Au polycrystalline electrode emersed from 0.1 M $NiSO_4$ electrolyte at various potentials.

TABLE 1: Nickel, Oxygen, and Carbon Surface Concentration of Electrochemically Deposited Nickel Adlayer on Gold Electrode, as Estimated by XPS Intensities[a]

	% nickel concentration	% oxygen concentration	% carbon concentration
−0.48 V	16	43	41
−0.55 V	34	46	20
−0.65 V	43	47	10
−0.65 to −1.2 V	41 ± 5%	48 ± 5%	11 ± 5%
$Ni(OH)_2$[b]	37.2	50.9	11.9

[a] Reference data for slightly hydrated $Ni(OH)_2$ are also shown for comparison. [b] Data were taken from ref 20.

and thus the aforementioned deconvolution method did not give reliable results. The rinsing procedure that followed sample emersion from the electrochemical cell does not influence the amount of water species adsorbed on the electrode. This assignment is supported by separate experiments, where the sample was emersed from the cell and was examined in UHV without rinsing in Millipore water. Line shape analysis of the overall O 1s peak (not shown) shows the existence of two oxygen species at 531.8 and 533.2 eV, the relative intensities of which were in agreement with those presented in Figure 7.

To evaluate the composition of the deposited film on the electrode, we calculated nickel and oxygen atomic concentration for various applied potentials and compared them to previously published values for $Ni(OH)_2$,[20] as listed in Table 1.

The atomic concentration of elements on the deposited film was estimated using a homogeneous layer model consisting of nickel, oxygen, and hydrocarbon impurities. Surface atomic ratios were calculated from XPS peak areas and atomic sensitivities[30] assuming uniform distribution of all elements. The atomic sensitivities obtained from reference[30] were corrected

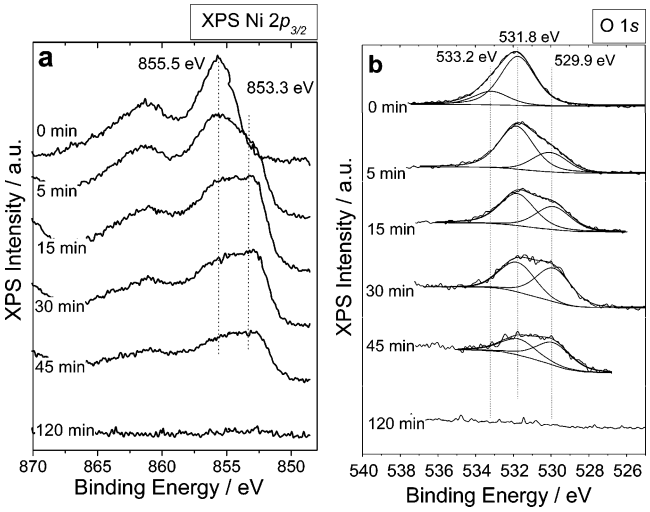

Figure 8. XP spectra of the (a) Ni $2p_{3/2}$ and (b) O 1s core levels for a Au polycrystalline electrode emersed at −0.65 V vs SCE from 0.1 M $NiSO_4$ electrolyte as a function of sputter time.

taking into account the measured energy dependence of our analyzer transmission. The calculated values obtained are dependent on the applied potential, at least for potentials up to −0.65 V. At higher potentials, the calculated atomic concentrations are closely related to those of nickel and oxygen in $Ni(OH)_2$ compound found previously. However, this is not the case for −0.48 and −0.55 V samples, where compounds rich in oxygen were found. In this respect, it can be concluded that the applied potential is decisive for the adsorbed nickel layer composition.

3.2.3. Ar Ion Sputtering Depth Profile. To learn more about the composition and spatial arrangement of the surface layer, sputter experiments with argon were performed. The sputter conditions were $P(Ar) = 3.1 \times 10^{-6}$ mbar; $E = 500$ eV, and Isp ~3 μA. The result of such a sputtering sequence is shown in Figure 8 for a Ni-covered Au electrode prepared after an immersion time of 170 s, at −0.65 V. Binding energies before the sputtering procedure were shifted, in accordance with what has been presented in Figure 4, and their energies were corrected by using C 1s peak as a reference. However, after mild sputtering this shift was eliminated and no charge correction was necessary. Initially, Ni $2p_{3/2}$ spectra (Figure 8a) exhibits a relatively narrow peak centered at 855.5 eV, similar to those presented in Figure 4. The chemical changes induced by Ar ion bombardment can be clearly observed. After 5 min of sputtering, a small shoulder appears about 2 eV below the main Ni $2p_{3/2}$ peak. After further ion exposure (15 min), the intensity of this shoulder increases and persists until Ni 2p signal completely vanishes after a total sputtering of 120 s. The low binding energy shoulder at ca. 853.3 eV can be attributed to a new Ni−O compound induced by the sputtering procedure,[11,28] whereas the initially presented $Ni(OH)_2$ peak never disappears completely in any of the sputtering steps.

The above picture was further confirmed by O 1s signal presented in Figure 8b. A careful peak shape analysis reveals that before sputtering the oxygen peak consists of two species, namely, OH and adsorbed H_2O, as described in Figure 7. Adsorbed H_2O species disappear very readily after 5 s sputtering time, followed by the emergence of a new peak at BE 529.9 eV. This peak is much more tenacious than the H_2O peak and its relative intensity increases upon further sputtering, following the same trend as the low binding energy shoulder of Ni $2p_{3/2}$ peak in Figure 8a. O 1s peaks at 529.9 ± 0.2 eV were previously

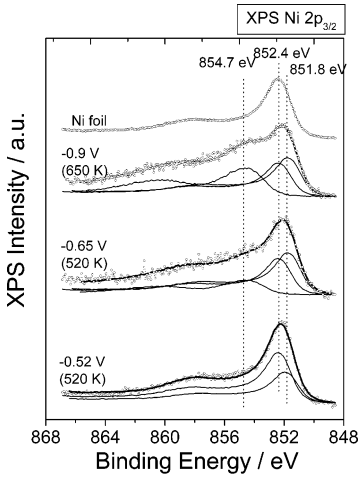

Figure 9. XP spectra of the Ni $2p_{3/2}$ core level for a Au polycrystalline electrode emersed at various potentials from 0.1 M $NiSO_4$ electrolyte and subsequently annealed in ultrahigh vacuum chamber up to 650 K. The spectrum of a reference polycrystalline Ni foil is also shown at the top of the figure.

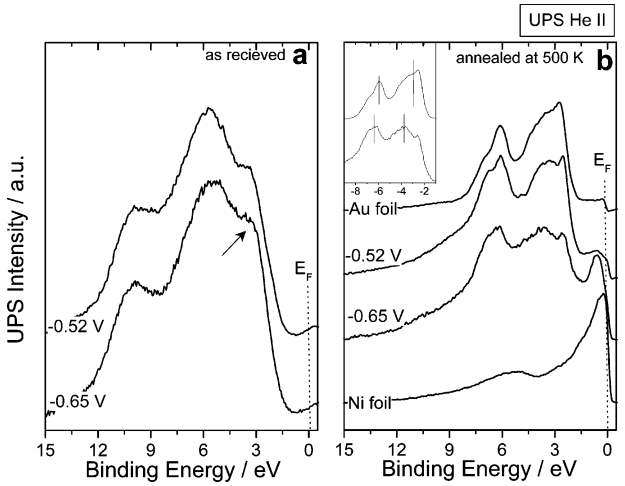

Figure 10. Helium II UP valence band spectra for a Au polycrystalline electrode emersed at −0.52 and −0.65 V from 0.1 M $NiSO_4$ electrolyte (a) before annealing (b) after annealing at 520 K in UHV. The UP spectrum of reference Au and Ni polycrystalline foils are also shown for comparison. Inset: Comparison of the Au 5d doublet between bulk Au and −0.65 V Ni/Au sample.

assigned to O in NiO[11,28] and its presence agrees very well with the appearance of the shoulder in lower binding energies in the Ni 2p spectrum. This strongly suggests that the O species at 529.9 eV are indeed directly linked to the Ni atoms inducing the low binding energy side shoulder at the Ni 2p signal. Since there is no evidence of the presence of NiO species among deposited $Ni(OH)_2$ in any of our experiments, the new NiO compound at the surface originates from the dissociation of OH−Ni−OH bonds induced by Ar ion bombardment. Decomposition of $Ni(OH)_2$ to NiO by an ion beam has been observed before for high purity nickel hydroxide powders.[31]

3.2.4. Sample Annealing in UHV. With the intention of determining the thermal stability of the nickel adlayer, the sample was annealed in UHV and then XPS measurements were carried out. Upon heating the sample, the hydroxide related species at Ni 2p and O 1s region gradually decline, followed by a decrease of the overall Ni/Au intensity ratio. Figure 9 shows the Ni $2p_{3/2}$ peaks after annealing for three Ni deposits at −0.52, −0.65 V, and −0.9 V. The corresponding spectrum from the reference Ni foil is also shown for comparison. Annealing the sample induces a new Ni $2p_{3/2}$ peak at 852.1 eV, which appears at the expense of the peak initially located at higher energies (see Figure 4). The shift of the Ni $2p_{3/2}$ peak at lower binding energies, as well as the attenuation of its satellite peak, can safely be assigned to the decomposition of nickel hydroxide toward nickel in its metallic form. This is true for all samples and is independent of the emersion potential and correlates well with previous studies, which indicates that OH groups desorb from hydroxidized nickel samples around 550 K.[24] In addition, a profound decrease between 20 and 50% of Ni/Au intensity ratio upon annealing indicates the shrinkage of initially deposited nickel film because of its agglomeration in larger particles. However, thicker nickel layers formed at more cathodic potential require higher temperatures for OH groups desorption.

The Ni $2p_{3/2}$ binding energy of the annealed electrodeposited nickel is 0.3 eV lower and exhibits increased fwhm compared to that of the clean Ni surface, measured using the same experimental apparatus under identical conditions. This 0.3 eV binding energy shift in the XP Ni 2p spectra of the annealed samples is consistent and reproducible in all annealing experiments. Curve fitting of the Ni $2p_{3/2}$ peak on the basis of line shape of clean metal reference spectra and thick oxidized film reveals the existence of three Ni $2p_{3/2}$ peaks. The intensity maxima of those peaks are found in binding energies of 852.4 ± 0.1, 851.8 ± 0.1, and 854.7 ± 0.2 eV (for −0.52 V only two components are necessary to fit the overall spectrum). As is evident, the 852.4 eV peak can be assigned to metallic nickel (Ni^0), whereas the peak at 854.7 eV, which is accompanied by a strong satellite peak, is most probably due to residual oxidized Ni species that remain on the surface after annealing. This was also confirmed by the small but detectable peak in O 1s region at 529.9 eV (not shown). The low-energy component at 851.8 ± 0.1 is shifted −0.6 eV versus metallic Ni and cannot be assigned to any oxidized form of nickel. This peak is evidence of intermetallic compound formation as will be discussed in section 4.

3.2.5. UPS Experiments. Additional information about the chemical state of the interface can be derived from the valence band configuration. A pair of spectra illustrating the valence band of the electrochemically deposited Ni on Au under −0.52 and −0.65 V together with a second set of spectra acquired after heating the sample at 520 K are given in Figure 10a and 10b, respectively. Reference spectra from clean Ni and Au surfaces are shown for comparison at the bottom and the top of Figure 10b. Before annealing the sample (Figure 10a), the valence band spectrum is dominated by intense density of states (DOS) centered at 3.5, 5.5, and 9.7 eV. Despite the complex nature of the valence band spectra, one can attribute the main features that appear in Figure 10a to surface characteristics associated to XPS measurements. The intense shoulder at ca. 3.5 eV in Figure 10a can be attributed to hydroxidized Ni 3d states, with a possible contribution of Au 5d states of the support. In addition, the DOS centered at ca. 5.5 and 9.7 eV is the fingerprint of the OH^- radicals.[32,33] We therefore attribute the high-binding energy peaks observed in Figure 10a mainly to photoemission from 1π and 3σ orbital of OH species, with a contribution of Au 5d states and possible inflection of DOS derived from residual hydrocarbon impurities.[34]

There is not any significant dependence of the valence band spectrum of Figure 10a on the applied potential, except for a small increase in the low binding energy states at −0.65 V (indicated by an arrow). This is probably due to an increased nickel hydroxide film thickness, as also pointed out from the XPS measurements (section 3.2.1). XPS has shown 4 times higher Ni/Au intensity ratio for −0.65 V, as compared to the

−0.52 V sample. However, this difference is not illustrated in UPS spectrum. This might be an indication of homogeneous $Ni(OH)_2$ layer, the thickness of which in both samples is comparable to the surface sensitivity of UPS (up to 10 ML).

Upon heating at 520 K, there is a reduction in the intensity of the OH^- features, accompanied by the appearance of characteristic Ni 3d states immediately below the Fermi level and the Au 5d doublet at ca. 3.2 and 6.2 eV. There are also residual hydroxyl groups noticeable between Au 5d components. It is also deduced by comparing the spectra at −0.52 and −0.65 V in Figure 10b that the position of Au 5d and Ni 3d states is not modified with changing the applied potential and they are identical to those measured in the reference samples. However, for the sample subjected to −0.52 V sample, there is an attenuation of the Ni 3d intensity at the Fermi edge (compared to −0.65 V sample), consistent with XPS data which show a significant increase in the Ni/Au intensity ratio of the −0.65 V sample. In this respect, UPS measurements are in line with the results derived from analysis of the core level peaks.

Evidence for alloy formation is provided by the difference valence band spectra, which emerge after the subtraction of the metallic nickel component of the overall valence band spectrum. The Au 5d band splitting decreases from 2.85 eV in the bulk Au metal to 2.6 eV for −0.65 V sample (see inset of Figure 10b). We do not however see significant changes in the splitting for −0.52 V sample, after the same procedure. Although changes in the Au 5d splitting for −0.65 V in difference spectra must be considered with care because of the addition of residual nickel hydroxide species, the observed shift in the Au 5d splitting is in accordance with previous findings for surface alloyed Au−Ni systems.[35] However, this shift in the Au 5d band is difficult to distinguish for small Ni coverages because of the intense signal contribution of the Au bulk, compared to surface alloyed atoms signal. This is probably the reason for undetectable changes in Au 5d band split found for the −0.52 V sample.

4. Discussion

4.1. Formation of Nickel Adlayer on Gold. The experimental results presented above reveal a detailed picture of the state of the emersed Au electrode with the electrodeposited Ni on it, as well as of the induced modifications of the film after annealing in UHV. The main outcome of the above-described results is the formation of a slightly hydrated $Ni(OH)_2$ film on the Au electrode by cathodic current application at electrode potentials more negative than −0.5 V versus SCE. The formation of Ni^0 starts at −0.8 V, where reduced and hydroxidized nickel phases coexist on the electrode surface.

The mechanism of Ni deposition and formation of hydroxide nickel adlayer must be associated to the basic chemical environment (increased pH), which is developed at the double layer because of the hydrogen evolution reaction. Therefore, the high concentration of diluted OH^- ions at the double layer region because of H_2 evolution induces the precipitation of nickel on the electrode surface as $Ni(OH)_2$ according to the following reaction:

$$Ni_{aq}^{2+} + 2H_2O + 2e^- \leftrightarrow Ni(OH)_2 + H_2 \qquad (1)$$

The Ni^0 co-deposition on the Au electrode observed at potentials below −0.8 V could be caused by the discharge of Ni^{2+} because of the charge-transfer reaction:

$$Ni_{aq}^{2+} + 2e^- \leftrightarrow Ni_{ad}^{0} \qquad (2)$$

The differences observed in growth mechanism upon potential changes suggest that the applied potential is decisive for deposited nickel chemical state. It is well established that no underpotential deposition of nickel on gold takes place from a $NiSO_4$ solution.[9] In other words, the onset of nickel layer formation on gold is observed at more cathodic potentials than that of the Ni^0/Ni^{2+} reversible Nerst potential (ca −0.75 V at 0.1 M $NiSO_4$ solution). It is now evident why the formation of nickel adlayer following reaction 2 is not thermodynamically favored at more positive potentials than −0.75 V. Nevertheless, for these potentials, that is, above −0.75 V, nickel deposition follows an alternative path, by precipitating in a hydroxide form (reaction 1) because of the strong basic environment within the double layer region. However, as it is evidently shown in Figure 4, the relative Ni^0/Ni^{2+} intensity ratio decreases when potential shifts toward more negative values. Taking into account that reactions 1 and 2 run in parallel, it looks likely that with increasing film thickness reaction 2 would be hindered, thus resulting in lower deposition rates of Ni^0 on the electrode surface. In addition, the attenuation of Ni^0 XPS signal can be attributed to the increase of the thickness of the $Ni(OH)_2$ overlayer, which probably surrounds the Ni^0 deposit.

Considering the voltammograms of Figure 2, the dissolution of Ni must follow the reversed reaction of reaction 1, which involves the abstraction of hydroxyl groups and the dissolution of Ni^{2+} ions in the solution. However, as was already mentioned, the development of a rather intense and narrow dissolution peak at −0.35 V upon polarization at higher cathodic potential and the existence of the broader peak at −0.1 V indicates the existence of more than one Ni chemical state. Taking into account the fact that upon increasing cathodic polarization the Ni 2p to O 1s XPS intensity ratio increases (see Table 1), it is possible that the stoichiometry of $Ni(OH)_2$ layer varies. In particular, the excess of Ni at more cathodic potentials is probably due to the accumulation of Ni^{2+} at the outer plane of the electrochemical double layer. In this respect, we can consider two nickel phases in different chemical environments that constitute the electrochemical double layer: (i) nickel in coordination with an excess of hydroxyls and (ii) Ni^{2+} ions which are accumulated in excess because of the effect of the electric field at the double layer. Water molecules found at the outermost of the double layer are most likely responsible for the passivity of the later nickel species. Thus, it is rather rational to attribute the more narrow and intense peak at −0.35 V to the accumulated Ni^{2+} ions while the broader dissolution peak with peak maximum around −0.1 V implies the dissociation of $Ni(OH)_2$.

4.2. Structure of the Double Layer. XPS investigations on emersed electrodes revealed that the core level binding energies of species that reside within the surface dipole layer, (such as specifically adsorbed ions), do not shift with applied potential, whereas those species outside the surface dipole layer, (such as nonspecifically adsorbed ions), do shift with applied potential.[22,36] The binding energy shifts for nonspecifically adsorbed ions track the emersion potential with a ratio of nearly 1:1, thus corresponding to the activation overpotential being developed during polarization of the interface.[12,13] However, for thick insulating films, charging effects during X-ray irradiation can also be responsible for such shifts, which actually become larger as the layer is getting thicker. It is difficult to distinguish between the two possible origins of Ni 2p binding energy shift. However, from Figure 5 it is rather evident that up to −0.8 V the increase of the Ni 2p binding energy versus applied potential, with unity slope, reflects the potential drop across the double

layer that nickel ions should feel in full. For more cathodic potentials, the observed shifts up to 5 eV toward higher binding energies of the Ni 2p, O 1s, and C 1s photoelectron spectra are mainly due to charging effects. As depicted in Figure 6, the subsequent exposure of the sample to the atmosphere after its initial polarization and transfer to UHV under N_2 resulted in the decrease of the binding energy of Ni 2p, O 1s, and C 1s toward lower binding energies by ca. 1.4 eV. This shift does not correspond to any modification in the chemical state of the corresponding species as the shape of their photoelectron spectra remains the same, but instead it may reflect increase in the electrical conductivity of the layer because of the increase of carbon deposits upon its exposure to the ambient air. On the other hand, as was clearly shown in Figures 4 and 6, the Ni 2p peak centered at ca. 852.4 eV remains unchanged at a fixed binding energy. Thus, it can be concluded that Ni^0 adsorbs directly onto the Au surface, forming a thin layer (possibly a monolayer) of adsorbed Ni on Au, above which the formation of nickel hydroxide takes place.

The existence of adsorbed water on the electrode was evident in the O 1s peak of Figures 7 and 8b. The shift in the binding energy of the water component in the overall O 1s peak with potential shows that the water molecules follow the trend of OH groups and hence are nonspecifically adsorbed on the gold electrode. The relative XPS intensity of the H_2O component (compared with that of OH component) decreases with Ni coverage (see Figure 7). However, the absolute intensity of the H_2O component does not change considerably and was found constant in a range of 18%. In thick nickel hydroxide films (e.g., at -0.65 V), lower relative XPS intensities for the H_2O oxygen species are expected, since the contribution of the O 1s signal associated with OH species is much more intense. For thinner Ni films (e.g., at -0.48 V), the surface to bulk atomic ratio increases, leading to an increase of the relative H_2O induced O 1s signal. In addition, mild sputtering induces the removal of H_2O component at the surface (Figure 8b), in contrast to OH ions which are much more tenacious. The results mentioned above demonstrate that H_2O molecules must be located mainly on the outermost surface layer, whereas OH species are associated with the total amount of nickel deposited.

4.3. Evidence of Ni−Au Surface Alloy Formation. The results of the annealing experiments presented in Figures 9 and 10b show that OH species disappear very readily, followed by a decrease in intensity of the Ni 2p peak. Those changes are accompanied by a complete collapse of the electrochemical double layer. A careful analysis of Ni $2p_{3/2}$ signal revealed a new component at 851.8 eV, which is independent of the initial Ni quantity. Traces of carbon that remained on the surface after heating cannot account for this peak (through a possible nickel carbide formation), since neither Ni 2p nor C 1s peaks show the expected 0 and -0.6 eV binding energy shift, respectively, described previously for such compounds.[37] The presence of the peak at 851.8 eV is in reasonable agreement with Au−Ni surface alloy formation. In Au−Ni surface alloys prepared by thermal deposition in UHV[35] or by rapid quenching of molten metals,[38] the Ni 2p peak undergoes a shift of -0.6 ± 0.1 eV with respect to the bulk metal value. UPS results are in accordance with the above picture, showing a decrease in Au 5d band splitting as has been observed before for Au−Ni intermetallic compounds.[35]

Because of localization of Au−Ni alloy formation on the first layer, it is difficult to resolve from the XP spectra whether this alloy is formed during electrodeposition or is formed after annealing the sample in UHV. However, the former is unlikely to happen at least for low potentials, since we do not observe any metallic-like state in XPS. Upon annealing and desorption of adsorbed species, the surface intermixing of Au−Ni atoms is a favorable process as previously supported by total energy calculations based on the effective-medium theory.[39]

5. Conclusions

In this work, combined electrochemical and photoemission studies were employed to investigate Ni deposition on a polycrystalline Au electrode from a Ni sulfate solution. The results show that Ni deposition is qualitatively and quantitatively controlled by the applied potential. Two Ni chemical species, a reduced and a hydroxidized one, were detected. The reduced species adsorb in direct contact with the electrode (specifically adsorbed), while the hydroxidized most probably precipitate on the electrode because of its strong basic chemical environment during cathodic polarization and H_2 evolution. Annealing the Ni deposited Au electrode in UHV leads to the formation of a Au−Ni surface alloy as determined by photoemission results.

Acknowledgment. This paper has been supported by and carried out within the EU Project "*Apollon*", Contract No. ENK5-CT-2001-00572, EU Project No. NNES-2001-00187, and EU Project "Prometheas", Contract No. ICA2-2001-10037.

References and Notes

(1) Maroun, F.; Ozanam, F.; Magnussen, O. M.; Behm, R. J. *Science* **2001**, *293*, 1811.
(2) Kolb, D. M. *Surf. Sci.* **2002**, *500*, 722.
(3) Saraby-Reintjes, A.; Fleischmann, M. *Electrochim. Acta* **1984**, *29*, 557.
(4) Chassaing, E.; Jousselin, M.; Wiart, R. *J. Electroanal. Chem.* **1983**, *157*, 75.
(5) Tadjeddine, A.; Lahrichi, A.; Tourillon, G. *J. Electroanal. Chem.* **1993**, *360*, 261.
(6) Zhou, M.; Myung, N.; Chen, X.; Rajeshwar, K. *J. Electroanal. Chem.* **1995**, *398*, 5.
(7) Moller, F. A.; Magnussen, O. M.; Behm, R. J. *Phys. Rev. Lett.* **1996**, *77*, 3165.
(8) Moller, F. A.; Magnussen, O. M.; Behm, R. J. *Phys. Rev. Lett.* **1996**, *77*, 5249.
(9) Moller, F. A.; Kintrup, J.; Lachenwitzer, A.; Magnussen, O. M.; Behm, R. J. *Phys. Rev. B* **1997**, *56*, 12506.
(10) Bubendorff, J. L.; Cagnon, L.; Costa-Kieling, V.; Bucher, J. P.; Allongue, P. *Surf. Sci.* **1997**, *384*, L836.
(11) Casella, I. G.; Guascito, M. R.; Sannazzaro, M. G. *J. Electroanal. Chem.* **1999**, *462*, 202.
(12) Hansen, W. N. *J. Electroanal. Chem.* **1983**, *150*, 133.
(13) Stuve, E. M.; Krasnopoler, A.; Sauer, D. E. *Surf. Sci.* **1995**, *335*, 177.
(14) Papaefthimiou, V.; Siokou, A.; Kennou, S. *J. Appl. Phys.* **2002**, *91*, 4213.
(15) Magnussen, O. M.; Behm, R. J. *J. Electroanal. Chem.* **1999**, *467*, 258.
(16) Fleischmann, M.; Saraby-Reintjes, A. *Electrochim. Acta* **1984**, *29*, 69.
(17) Benje, M.; Eiermann, M.; Pittermann, U.; Weil, K. G. *Ber. Bunsen-Ges. Phys. Chem.* **1986**, *90*, 435.
(18) Soriaga, M. P. *Prog. Surf. Sci.* **1992**, *39*, 325.
(19) Kelber, J.; Seshadri, G. *Surf. Interface Anal.* **2001**, *31*, 431.
(20) Mansour, A.; Melendres, C. A. *Surf. Sci. Spectra* **1996**, *3*, 247.
(21) Mansour, A.; Melendres, C. A. *Surf. Sci. Spectra* **1996**, *3*, 271.
(22) Kotz, E. R.; Neff, H.; Muller, K. *J. Electroanal. Chem.* **1986**, *215*, 331.
(23) Shalvoy, R. B.; Reucroft, P. J.; Davis, B. H. *J. Catal.* **1979**, *56*, 336.
(24) de Jesus, J. C.; Carrazza, J.; Pereira, P.; Zaera, F. *Surf. Sci.* **1998**, *397*, 34.
(25) Yih-Wen Chen, D.; Noufi, R. *J. Electrochem. Soc.* **1984**, *131*, 1447.
(26) Zafeiratos, S.; Kennou, S. *Surf. Sci.* **2001**, *482−485*, 266.
(27) Luo, P. F.; Kuwana, T.; Paul, D. K.; Sherwood, P. M. *Anal. Chem.* **1996**, *68*, 3330.
(28) Kitakatsu, N.; Maurice, V.; Hinnen, C.; Marcus, P. *Surf. Sci.* **1998**, *407*, 36.
(29) Pirug, G.; Knauff, O.; Bonzel, H. P. *Surf. Sci.* **1994**, *321*, 58.

(30) *Practical Surface Analysis*, 2nd ed.; Briggs, D., Seah, M. P., Eds.; Wiley: New York, 1990; Vol. 1, p 201.
(31) Chuang, T. J.; Brundle, C. R.; Wandelt, K. *Thin Solid Films* **1978**, *53*, 19.
(32) Mckay, J. M.; Henrich, V. E. *Phys. Rev.* **1985**, *B32*, 6734.
(33) De Asha, A. M.; Critchley, J. T. S.; Nix, P. M. *Surf. Sci.* **1988**, *405*, 201.
(34) Kirstein, W.; Petraki, I.; Thieme, F. *Surf. Sci.* **1995**, *333*, 162.
(35) Santra, A. K.; Rao, C. N. R. *Appl. Surf. Sci.* **1995**, *84*, 347.
(36) D'Agostino, A. T.; Hansen, W. *Surf. Sci.* **1986**, *165*, 268.
(37) Sinharoy, S.; Levenson, L. L. *Thin Solid Films* **1978**, *53*, 31.
(38) Fuggle, J. C.; Hillebrecht, F. U.; Zeller, R.; Zolnierek, Z.; Bennet, P. A.; *Phys. Rev. B* **1982**, *27*, 2145.
(39) Pleth Nielsen, L.; Besenbacher, F.; Stensgaard, I.; Laegsgaard, E.; Enghahl, C.; Stoltze, P.; Jacobsen, K. W.; Norskov, J. K. *Phys. Rev. Lett.* **1993**, *71*, 754.